ACS Catalysis

Research Article

pubs.acs.org/acscatalysis

Density Functional Theory-Computed Mechanisms of Ethylene and Diethyl Ether Formation from Ethanol on γ-Al_2O_3(100)

Matthew A. Christiansen, Giannis Mpourmpakis, and Dionisios G. Vlachos*

Department of Chemical and Biomolecular Engineering, Catalysis Center for Energy Innovation and Center for Catalytic Science and Technology, University of Delaware, Newark, Delaware 19716-3110, United States

Supporting Information

ABSTRACT: Multiple potential active sites on the surface of γ-Al_2O_3 have led to debate about the role of Lewis and/or Brønsted acidity in reactions of ethanol, while mechanistic insights into competitive production of ethylene and diethyl ether are scarce. In this study, elementary adsorption and reaction mechanisms for ethanol dehydration and etherification are studied on the γ-Al_2O_3(100) surface using density functional theory calculations. The O atom of adsorbed ethanol interacts strongly with surface Al (Lewis acid) sites, while adsorption is weak on Brønsted (surface H) and surface O sites. Water, a byproduct of both ethylene and diethyl ether formation, competes with ethanol for adsorption sites. Multiple pathways for ethylene formation from ethanol are explored, and a concerted Lewis-catalyzed elimination (E2) mechanism is found to be the energetically preferred pathway, with a barrier of E_a = 37 kcal/mol at the most stable site. Diethyl ether formation mechanisms presented for the first time on γ-Al_2O_3 indicate that the most favorable pathways involve Lewis-catalyzed S_N2 reactions (E_a = 35 kcal/mol). Additional novel mechanisms for diethyl ether decomposition to ethylene are reported. Brønsted-catalyzed mechanisms for ethylene and ether formation are not favorable on the (100) facet because of weak adsorption on Brønsted sites. These results explain multiple experimental observations, including the competition between ethylene and diethyl ether formation on alumina surfaces.

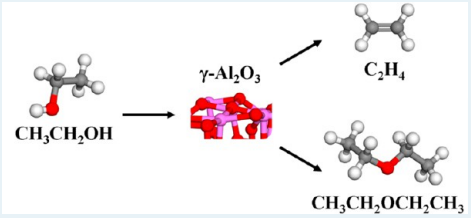

KEYWORDS: *γ-Al_2O_3, ethanol, dehydration, etherification, ethylene, diethyl ether, Lewis acid, DFT*

INTRODUCTION

γ-Al_2O_3 is widely used in heterogeneous catalysis as a support material because of its good thermal stability and high surface area,[1] and as a washcoat in automobile catalytic converters.[2] γ-Al_2O_3 itself also demonstrates activity for several reactions including the Claus process for sulfur removal,[3] alkene double bond isomerization,[4] and dehydration of alcohols.[5] The interest in dehydration chemistry has expanded in recent years, as it represents one important route for removing oxygen from biomass-derived compounds.[6] Understanding the origin of dehydration by solid acids, such as γ-Al_2O_3, is the first step toward rational development of materials with superior catalytic properties.

While the activity of γ-Al_2O_3 for alcohol dehydration has been known for some time,[5] there are still significant research efforts aimed at understanding essential aspects of the active site(s) and reaction mechanisms.[7−13] In γ-Al_2O_3, bulk Al atoms display either tetrahedral or octahedral coordination. Exposed surface Al sites can display three-, four-, or 5-fold coordination (see for example ref 14 and references therein), and exhibit Lewis acidity. Depending on the preparation method and catalyst operating conditions, the γ-Al_2O_3 surface is often at least partially hydrated and/or hydroxylated, creating potential Brønsted sites. The role of different active sites in alcohol dehydration is debated. Pines and Haag applied a variety of probe molecules and indicators to study the surface, and concluded that Lewis sites are the dominant source of acidity.[15] In contrast, Knözinger et al. proposed that alcohols adsorb via hydrogen bonding to Brønsted sites.[16] More recently, Kwak et al. reported that Brønsted-bound ethanol is dehydrated to ethylene for catalysts calcined below 473 K, while ethylene originates from ethanol adsorbed on Lewis sites for catalysts treated above 673 K.[8] On the other hand, Roy et al. did not detect any evidence of Brønsted sites using catalysts treated at 573 K or higher, and they concluded that exposed Al surface sites (Lewis centers) are the primary adsorption sites for ethanol that lead to ethylene formation.[11]

Apart from the type and role of the acid sites in alcohol dehydration, there has also been substantial work on the reaction mechanism. Knözinger and Köhne were among the first to systematically examine the dehydration pathways leading to ethers and olefins.[17,18] They demonstrated that only ethers form at low temperatures (488 K), while olefins form at higher temperatures (616 K), either directly from the alcohol or via ether decomposition, or both.[17,18] Multiple experimental studies report a kinetic isotope effect (KIE) involving C−H bonds in olefin formation, and propose elimination-type mechanisms (either E1 or E2) to explain the observations.[13,19,20] Experiments on ether formation indicate that a bimolecular nucleophilic substitution (S_N2) mechanism

Received: April 15, 2013
Revised: July 11, 2013
Published: August 1, 2013

is active.[21−23] In addition to these studies, computational methods have also been applied to explore alcohol dehydration on alumina. Using density functional theory (DFT) calculations, both E1 and E2 concerted mechanisms have been proposed for olefin formation.[7,9,11] Two of these studies focused on butanol dehydration on the (100) facet.[7,9] The other work examined dehydration of various alcohols on a Al_8O_{12} cluster model with a tricoordinate Al site, which resembles the local environment of tricoordinate Al on γ-Al_2O_3(110);[11] the tricoordinated Al surface atoms have been reported to be strong Lewis acid-type catalytic sites.[24] Existing computational studies of ether formation from alcohols on γ-Al_2O_3 are limited. To our knowledge, only one DFT study of methanol dehydration on the (110) facet has been reported according to which dimethyl ether forms via reaction of two CH_3O groups.[10]

To improve our understanding of both the role and the nature of the active site(s) and the associated mechanisms for alcohol chemistry on γ-Al_2O_3, we have performed DFT calculations for dehydration and etherification reactions of ethanol on the (100) facet of γ-Al_2O_3. We are not aware of any previous DFT study examining ethanol dehydration on this facet, which contains pentacoordinated sites. Such pentacoordinate sites are observed to be experimentally active for ethanol dehydration,[8,25] motivating us to explore the (100) facet. We explore multiple pathways for ethylene formation including novel ether decomposition mechanisms and, to the best of our knowledge, we report the first DFT-computed diethyl ether formation mechanisms on γ-Al_2O_3. Both Lewis- and Brønsted-catalyzed mechanisms are considered in this study.

COMPUTATIONAL METHODS

The Vienna Ab initio Simulation Package (VASP)[26−29] was used to perform the calculations. We employed the PW91 functional developed by Perdew and Wang utilizing the generalized gradient approximation (GGA),[30,31] and pseudopotentials developed using the projector augmented wave (PAW) method.[32,33] The PAW pseudopotentials were used as distributed by VASP (standard version of the potential for each element in our system). We simulated the (100)-2 × 1 surface using a supercell containing 80 atoms (corresponding to 4 atomic layers) with 15 Å of vacuum between periodic slabs, based on the nonspinel model for the bulk structure of γ-Al_2O_3 that was originally developed by Raybaud, Sautet, and coworkers.[34,35] Note that the (100) is the lowest-energy fully dehydrated facet reported for this alumina model.[35] The bottom atomic layer was held fixed in the bulk positions while all other atoms were allowed to relax. Consistent with previous literature,[35] surface relaxation has little effect on the atomic positions; the maximum vertical relaxation of unconstrained atoms is 0.15 Å, or 2% of the slab thickness. To assess the convergence of adsorption properties, results were compared to calculations of a 2 × 1 surface with the thickness doubled (an additional 80 atoms). The tested adsorption properties on the smaller slab were within 1 kcal/mol of the properties on the larger slab, when either the bottom two atomic layers or the entire bottom set of 80 atoms in the larger slab were kept fixed. The surface Brillouin zone was sampled using a 3 × 3 × 1 gamma-centered k-point grid. The plane wave basis set had a cutoff of 400 eV, and the forces in all calculations were converged to within 0.05 eV/Å (1.2 kcal/(mol Å)). Transition states (TSs) were located with either the climbing image nudged elastic band (CI-NEB) or Dimer methods.[36,37] These methods are often used in combination as described in ref 38.

ADSORBATE STABILITY AND STRUCTURE

The selection of the approach for computing adsorption energies on oxides merits careful consideration. Previous work has shown that the adsorption energy of Lewis acid−base adsorbate pairs on oxide surfaces is much stronger than the sum of the adsorbate energies of the isolated compounds.[39−41] The origin of this effect has been attributed to charge transfer between the adsorbates through the support, and it has been shown that this effect is suppressed by performing spin-constrained calculations.[39] Consistent with those findings, we observe on γ-Al_2O_3 a substantial decrease in the total energy when coadsorption takes place between ethoxy and atomic hydrogen radicals, and also between hydroxyl and hydrogen radicals (see Supporting Information, Table S1). The pairs of these radicals (each one carrying one unpaired electron) prefer to form a closed shell in the coadsorbed state (see Supporting Information, Table S1). We also performed a Bader charge analysis[42] to examine the charges on atomic hydrogen and hydroxyl adsorbates. We find that for the singlet (triplet) state, an additional electron density of 0.2 (0.1) $|e^-|$ is transferred to adsorbed OH from the surface in the presence of adsorbed H, compared to the case of adsorbed OH without any coadsorbate (see Supporting Information, Table S2). The amount of transferred charge in both spin states is similar. This suggests that, for this system, the change in spin states when comparing isolated adsorption with coadsorption (rather than the charge transfer) has a significant contribution to the total energy of the coadsorbed case. As a result of these observations, all calculations in this work utilize sets of adsorbates that are capable of forming closed-shell molecules without any leftover fragments so that the most stable adsorption states are used.

Figure 1 displays the (100)-2 × 1 surface used for the calculations of this work. The four Al atoms exposed on the

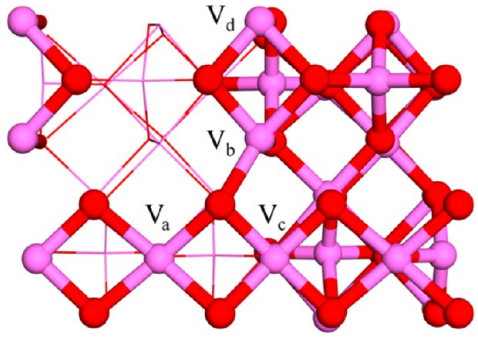

Figure 1. Top view of the γ-Al_2O_3(100)-2 × 1 surface. Al atoms shown in pink, O atoms in red. The "V_x" labels refer to the different Al sites and "V" stands for the coordination number. The subsurface atoms on the left side of the figure are drawn differently so that the surface atoms are more easily identified.

(100) plane (per unit area) are classified as pentacoordinated sites, whereas the six O atoms are tricoordinated. Site identifiers for Al and O sites are found in Figure 1 and Supporting Information, Figure S1. In the superscript, we use a site identifier to indicate on which type of site an adsorbate sits (e.g., $H_2O^{V_a}$ indicates water sits on the Al V_a site, H^O or $H^{O'}$ means atomic hydrogen is on an oxygen site). While all sites of a given element have the same coordination, they do not

dx.doi.org/10.1021/cs4002833 | ACS Catal. 2013, 3, 1965−1975

exhibit equivalent properties in terms of adsorption strength, electronic structure, and so on (particularly the Al sites).[35] Therefore, ethanol was selected as a probe molecule to examine adsorption on all 10 sites. The results for adsorption on the Al sites are presented in Table 1. Ethanol adsorbs through its oxygen in the alcohol group on the Lewis acidic Al sites. The strongest adsorption occurs on the Al V_a site with $\Delta E_{ads} = -19$ kcal/mol, while it is −14 kcal/mol on sites V_b and V_d and −10 kcal/mol on site V_c. When adsorbed over a surface O site, the hydrogen in the alcohol group is oriented toward the surface.

Table 1. Energy of Adsorption of Stable Gas-Phase Intermediates Adsorbed at Al Sites on the γ-Al_2O_3(100) Surface[a]

	ΔE_{ads} [kcal/mol]			
adsorbate	site V_a	site V_b	site V_c	site V_d
H_2O^{Al}	−20	−15	−13	−15
$C_2H_4^{Al}$	−4	−2	−2	−1
CH_3CHO^{Al}	−13	−5	−8	−4
$CH_3CH_2OH^{Al}$	−19	−14	−10	−14
$CH_3CH_2OCH_2CH_3^{Al}$	−12	−9	−8	−9

[a]Refer to Figure 1 for site identification. Adsorption energies are defined with respect to the corresponding molecule in the gas phase.

The adsorption energies, listed in Supporting Information, Table S3, range from −2 to −5 kcal/mol, consistent with a hydrogen bonding type of interaction. The adsorption energies for the other four stable gas-phase intermediates (water, ethylene, acetaldehyde, and diethyl ether) are reported for the Al sites (see Table 1). Similar to ethanol, they weakly interact with surface O sites. Although acetaldehyde is a dehydrogenation product, we include it to compare activation barriers of dehydration and dehydrogenation on alumina. The qualitative trends of relative binding strength on each Al site are consistent for ethanol, water, and diethyl ether. This means that the differences in adsorption strength on the various Al sites are due to electronic effects. Acetaldehyde differs slightly from other adsorbates in that it binds more strongly to the V_c site than to V_b and V_d (by 3 kcal/mol). All four oxygen-containing intermediates bind strongest to the V_a site. Ethylene binds weakly to all Al sites. Structures of these intermediates in their most stable configurations are found in Figure 2. Also, as shown in Table 1, water and ethanol have similar adsorption energies on all Al sites. This indicates that water and ethanol will compete for adsorption sites on the (100) surface. This is consistent with experimental observations that water strongly inhibits ethanol dehydration and etherification.[13]

Figure 2 and Figure 3 contain the structures of all intermediates considered in the network in their most stable

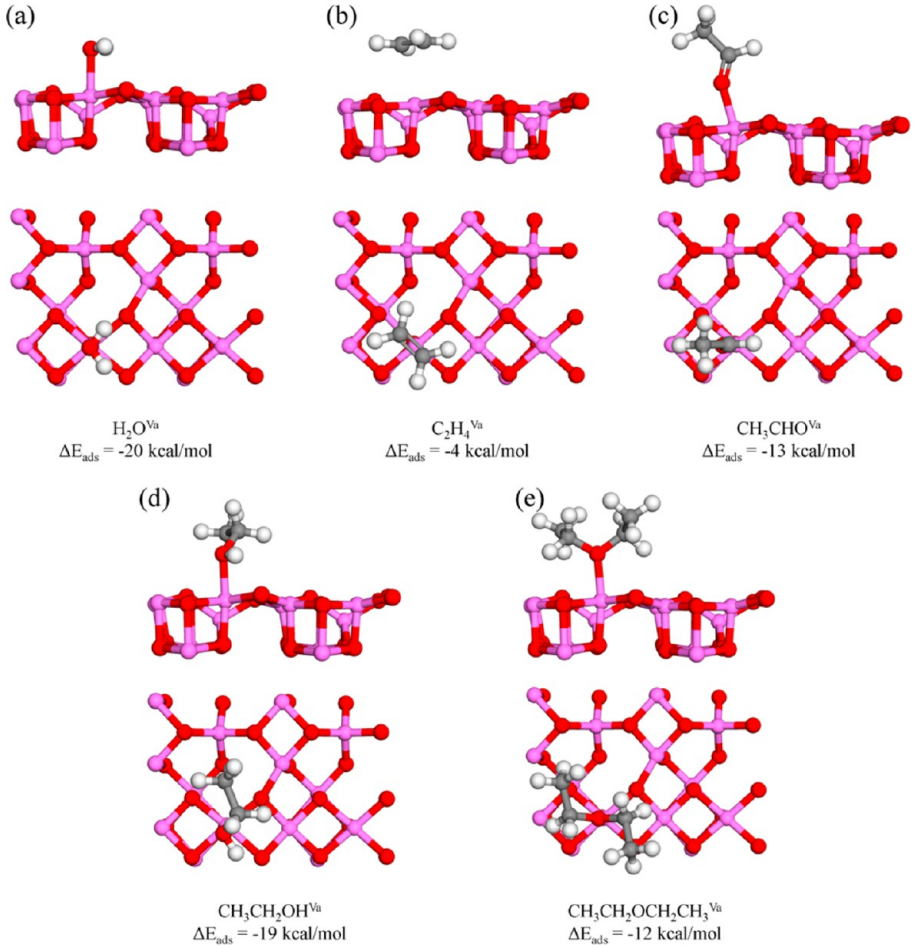

Figure 2. Structures and adsorption energies of the stable gas-phase intermediates of the ethanol reaction network in their most stable adsorbed configurations. (a) water, (b) ethylene, (c) acetaldehyde, (d) ethanol, (e) diethyl ether. Adsorption energies are defined with respect to the corresponding molecule in the gas-phase.

dx.doi.org/10.1021/cs4002833 | ACS Catal. 2013, 3, 1965−1975

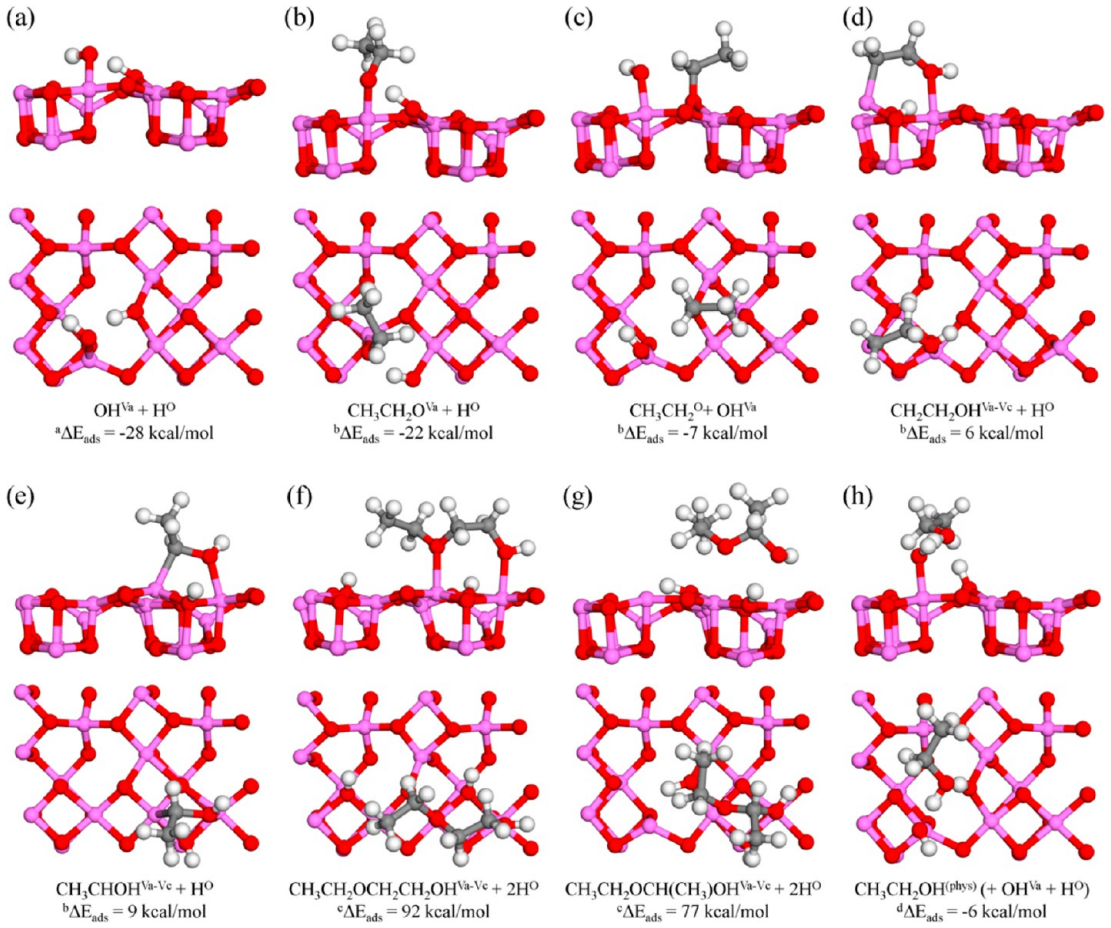

Figure 3. Structures of surface intermediates of the ethanol reaction network in their most stable adsorbed configurations. The adsorption energy of the featured adsorbate is listed adjacent to each subfigure with respect to a suitable reference. [a]Reference is $H_2O(g)$. [b]Reference is $CH_3CH_2OH_{(g)}$. [c]Reference is 2 $CH_3CH_2OH_{(g)}$. [d]Reference is $CH_3CH_2OH_{(g)}$ and OH^{Va} + H^{O} preadsorbed on the Al_2O_3 slab.

configurations. We examined different conformations of adsorbates, and found that differences in adsorption energies arising primarily from hydrogen bonding were on the order of 4 kcal/mol or less. Alongside each subfigure, the energy of the featured adsorbate is listed with respect to a suitable reference (adsorbate in the gas-phase for Figure 2; for Figure 3, see caption). The reference state for many of the adsorbates in Figure 3 is either one or two gas-phase ethanol molecules, to examine the energetic preference to form these adsorbates from the reactant ethanol. The stability of both the OH^{Va} + H^{O} and $CH_3CH_2O^{Va}$ + H^{O} adsorbed states is similar to (respectively) H_2O^{Va} and $CH_3CH_2OH^{Va}$ (see Figure 3(a)-(b)). OH^{Va} + H^{O} is more stable than H_2O^{Va} by 8 kcal/mol, while $CH_3CH_2O^{Va}$ + H^{O} is more stable than $CH_3CH_2OH^{Va}$ by 3 kcal/mol. In the dissociated states, there is hydrogen bonding between the R-O^{Al} group and H^{O}. The surface is also reconstructed upon dissociation, especially in the case of OH^{Va}, to accommodate hydrogen bond formation (see Figure 3(a)). The formation of ethyl and hydroxyl ($CH_3CH_2^{O}$ + OH^{Va}) relative to gas-phase ethanol is also stable (−7 kcal/mol), but not as stable as $CH_3CH_2O^{Va}$ + H^{O} (22 kcal/mol) or $CH_3CH_2OH^{Va}$ (19 kcal/mol). The surface O atom on which $CH_3CH_2^{O}$ is adsorbed is deflected upward from its starting position (see Figure 3(c)). All other adsorbates are less stable than their gas-phase reference (adsorption energies quantified in Figure 3). CH_3CHOH^{Va-Vc} and $CH_2CH_2OH^{Va-Vc}$ bind on two Al sites with one C−Al bond each. The Al atom to which carbon binds (V_c site) is shifted upward to reduce the strain induced by cyclization with the surface (see Figure 3(d)−(e)). $CH_3CH_2OCH_2CH_2OH^{Va-Vc}$ and $CH_3CH_2OCH(CH_3)OH^{Va-Vc}$ were explored as possible intermediates for ether formation. Their binding configurations were chosen based on the most stable adsorption of the precursors $CH_2CH_2OH^{Va-Vc}$ and CH_3CHOH^{Va-Vc}, respectively. They are both much less stable than the gas-phase reference (2 $CH_3CH_2OH(g)$, see Figure 3(f)−(g)) and are not likely intermediates for diethyl ether. Finally, to test the effect that H^{O} (a Brønsted acid) may have on catalyzing dehydration when some Al (Lewis) sites are blocked by water (in the form of OH^{Va} + H^{O}), an adsorbed state of ethanol was considered that interacts with both OH^{Va} and H^{O} via hydrogen bonding (see Figure 3(h)). Accounting for the fact that OH^{Va} and H^{O} are preadsorbed on the surface (and therefore that the hydrogen bond between those two species must break), the adsorption energy of ethanol is −6 kcal/mol, which is fairly weak compared to ethanol adsorption on Lewis sites. This is consistent with weak binding of N_2 and CO probe molecules to Brønsted sites.[24,35]

The discussion in previous paragraphs has focused on isolated intermediates and dissociation products of those intermediates. Recent studies have shown how adsorbate dimers inhibit dehydration rates on the γ-Al_2O_3 surface,[13] indicating that consideration of coadsorption effects is important. Co-adsorption of two ethanol molecules has been tested on distinct pairs of Al sites, namely, (1) V_a + V_b sites, and

dx.doi.org/10.1021/cs4002833 | ACS Catal. 2013, 3, 1965−1975

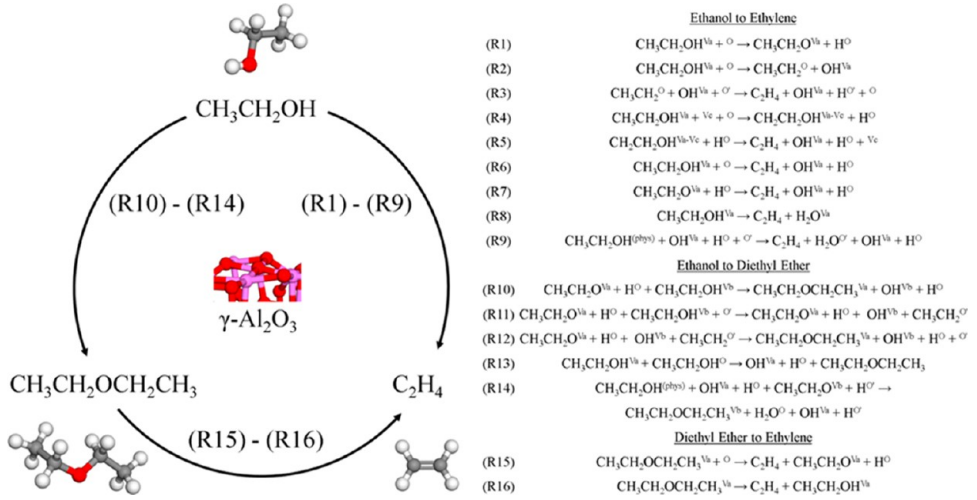

Figure 4. Reaction network for the production of diethyl ether and ethylene.

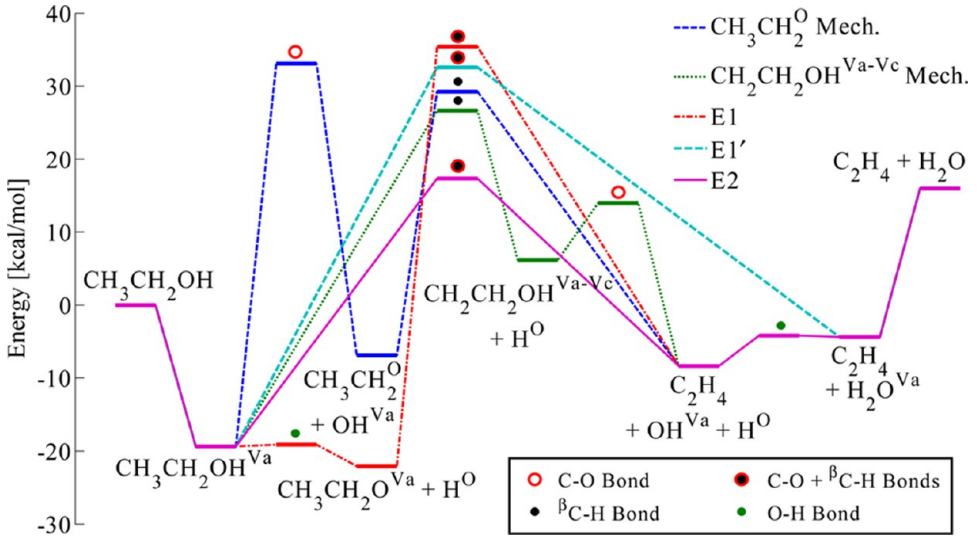

Figure 5. Energy diagram of principal reaction pathways for ethylene formation from ethanol. Each transition state is labeled to identify the bond(s) involved in the reaction.

(2) $V_a + V_c$ sites. We find that the adsorption energies of these "dimers" are virtually unchanged relative to the isolated adsorbates. For case (1), the adsorption energy of the coadsorbed state (relative to 2 ethanols in the gas phase) is −30 kcal/mol, whereas the sum of the binding energies of the isolated adsorbates is (using values from Table 1) −33 kcal/mol. For case (2), the adsorption energy of the coadsorbed state is −27 kcal/mol, whereas the sum of the binding energies of the isolated adsorbates is −29 kcal/mol. Therefore, we find no evidence of stabilizing effects from dimer formation on this facet. Similar to this, Digne et al.[35] (see inset to Figure 7a in ref 35) have found that increasing the water coverage on the (100) facet results in either an invariant or a decreasing differential adsorption energy. This indicates that stabilizing interactions indicative of water dimer formation are not observed on this facet. On the basis of these observations for ethanol−ethanol and water−water interactions, we do not expect that coadsorption of ethanol and water molecules will lead to significant stabilizing interactions. Further, dimers formed by ethanol and/or water adsorption involving the same Lewis center are not expected to be favorable on pentacoordinate sites because the Al becomes 6-coordinate after the first adsorbate binds. Dimer formation may be important on facets other than (100).

REACTION ENERGETICS AND KINETICS

The global reactions for the ethanol reaction network are shown in eqs 1−2

$$CH_3CH_2OH \rightarrow C_2H_4 + H_2O \quad (1)$$

$$2CH_3CH_2OH \rightarrow CH_3CH_2OCH_2CH_3 + H_2O \quad (2)$$

The elementary steps of (1) and (2) considered in this work are summarized in Supporting Information, Table S4, while Figure 4 contains an overview of the reaction network. The elementary steps listed in Figure 4 are numbered, and these numbers are used to reference the appropriate reaction in the discussion.

O−H Bond Scission and Formation. For both ethylene and ether formation, reactions involving O−H bonds are necessary to complete a catalytic cycle. O−H scission of both water and ethanol was explored and was found to be exothermic on V_a sites and slightly endothermic on other

dx.doi.org/10.1021/cs4002833 | ACS Catal. 2013, 3, 1965−1975

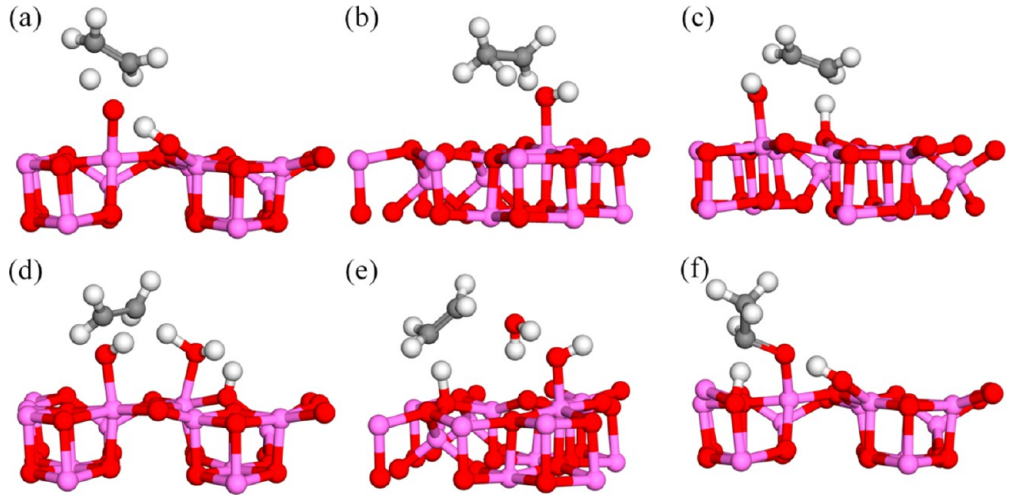

Figure 6. Transition state structures for ethylene and acetaldehyde formation from either ethanol or ethoxy. See Supporting Information, Table S2 and the text for energetic information. (a) $CH_3CH_2O^{Va} + H^{O} \rightarrow C_2H_4 + OH^{Va} + H^{O}$ (R7), (b) $CH_3CH_2OH^{Va} \rightarrow C_2H_4 + H_2O^{Va}$ (R8), (c) $CH_3CH_2OH^{Va} + {}^{O} \rightarrow C_2H_4 + OH^{Va} + H^{O}$ (R6), (d) $CH_3CH_2OH^{Va} + OH^{Vb} + H^{O} \rightarrow C_2H_4 + H_2O^{Vb} + OH^{Va} + H^{O}$, (e) $CH_3CH_2OH^{(phys)} + OH^{Va} + H^{O} + {}^{O\prime} \rightarrow C_2H_4 + H_2O^{O} + OH^{Va} + H^{O\prime}$ (R9), (f) $CH_3CH_2O^{Va} + H^{O} + {}^{Vc} + {}^{O} \rightarrow CH_3CHO^{Va\text{-}Vc} + 2H^{O}$.

sites (see Supporting Information, Table S4). Multiple attempts to locate transition states for these steps were unsuccessful, even after optimizing the intermediates so that the forces on all atoms were less than 0.01 eV/Å. The fact that the H in the R−OH group strongly interacts with (and is in close proximity to) the surface O site is consistent with a very low barrier or no barrier for O−H bond scission. This observation is similar to results of NEB calculations performed for (dissociated) water desorption on the γ-Al_2O_3(110) surface, in which no barriers were located.[43] Based on this result, and the fact that the stability of $CH_3CH_2OH^{Va}$, H_2O^{Va} and their O−H dissociation products are similar on sites V_b, V_c and V_d, we did not attempt to locate barriers on sites V_c and V_d for O−H scission reactions.

Ethylene Formation from Ethanol. To convert ethanol (or ethoxy) to ethylene, the C−O and $^{\beta}$C−H bonds of ethanol must break, leading naturally to a rehybridization of the carbon atoms and formation of the C−C double bond. The elementary steps involve either sequential or simultaneous scission of these bonds. We focus first (and primarily) on Lewis-catalyzed mechanisms. The energetics for five different pathways are plotted in Figure 5. In the "$CH_3CH_2{}^{O}$ mechanism" (R2)-(R3), the C−O bond first breaks via a barrier of 52 kcal/mol, and $^{\beta}$C−H scission of $CH_3CH_2{}^{O}$ occurs subsequently with a 36 kcal/mol barrier (Supporting Information, Figure S2(a)-(b)). In the "$CH_2CH_2OH^{Va\text{-}Vc}$ mechanism" (R4)-(R5), first $^{\beta}$C−H and then C−O scission occurs with a barrier of, respectively, 46 and 8 kcal/mol (Supporting Information, Figure S2(c)-(d)). The other three pathways involve concerted bond-breaking mechanisms. In the "E1" pathway (R1) and (R7), the O−H bond breaks to form $CH_3CH_2O^{Va}$, and then the $^{\beta}$H is transferred to the O of $CH_3CH_2O^{Va}$ while the C−O bond is broken. The barrier is 57 kcal/mol (Figure 6(a)). The "E1′" pathway (R8) involves a similar mechanism except that there is no initial O−H scission, and ethylene and H_2O^{Va} form directly from ethanol with a barrier of 52 kcal/mol (Figure 6(b)). In the "E2" pathway (R6), the $^{\beta}$H is abstracted by a surface O site as the C−O bond breaks, and the barrier is 37 kcal/mol (Figure 6(c)). Note that the terms "E1" and "E2" are indicative of the molecularity of the rate expression, including surface sites. For example, the E2 pathway (R6) is an elimination mechanism with two reactants involved in the forward rate expression ($CH_3CH_2OH^{Va}$ and a vacant O site). The E1 pathway (R7) has only one reactant ($CH_3CH_2O^{Va}$) participating in the forward rate expression; H^{O} is present but not involved in the reaction.

The E1 pathway via $CH_3CH_2O^{Va}$ (R7) is similar to a pathway proposed for 2-butanol dehydration, for which the reported barrier was ~26 kcal/mol.[9] This barrier is much lower than the one computed herein for ethanol (57 kcal/mol). Dispersion effects were found to be important for 2-butanol dehydration barriers,[9] but tests on our system revealed that barriers changed by less than 2 kcal/mol between calculations with and without dispersion. Our previously reported barrier for the E1 pathway on the alumina cluster exposing tricoordinated sites was 69 kcal/mol,[11] which is higher than that found in the present work. The E2 pathway (R6) is identical to the dehydration mechanism we reported previously,[11] and the barriers are very similar (within 5 kcal/mol). The E2 pathway is also similar to E2 mechanisms proposed by Dabbagh et al. for 2-butanol dehydration, though the lowest barrier they reported was 47 kcal/mol.[7]

From an energetic standpoint, the E2 mechanism (R6) is preferred for ethylene formation. For comparison, the pathway (R4) with the second-smallest barrier (forming $CH_2CH_2OH^{Va\text{-}Vc}$) is 46 kcal/mol. That results in a nearly 3 orders-of-magnitude difference in the rate constant (assuming an Arrhenius expression, equal values of the pre-exponential factor, and 500 K). The mechanism is also consistent with proposed mechanisms from literature and with observed KIEs for alcohols including ethanol.[13,19,20] Based on the favorable energetics, other mechanisms were examined in connection with the E2 path. The initial E2 barrier was computed using ethanol adsorbed on the Al V_a site. The calculation was repeated on the second-most stable Al site V_b, and the resulting barrier was nearly identical (different by 1 kcal/mol), showing that the barrier is not particularly site-dependent. This is consistent with our reported correlation of the activation barrier of alcohol dehydration with the carbenium ion stability of the reacting molecule.[11] Since the reaction barrier is mainly determined by the property of the alcohol (carbenium ion stability) and there is no significant change in the Lewis acidity of the Al sites (all are pentacoordinated sites), we expect similar

dx.doi.org/10.1021/cs4002833 | ACS Catal. 2013, 3, 1965−1975

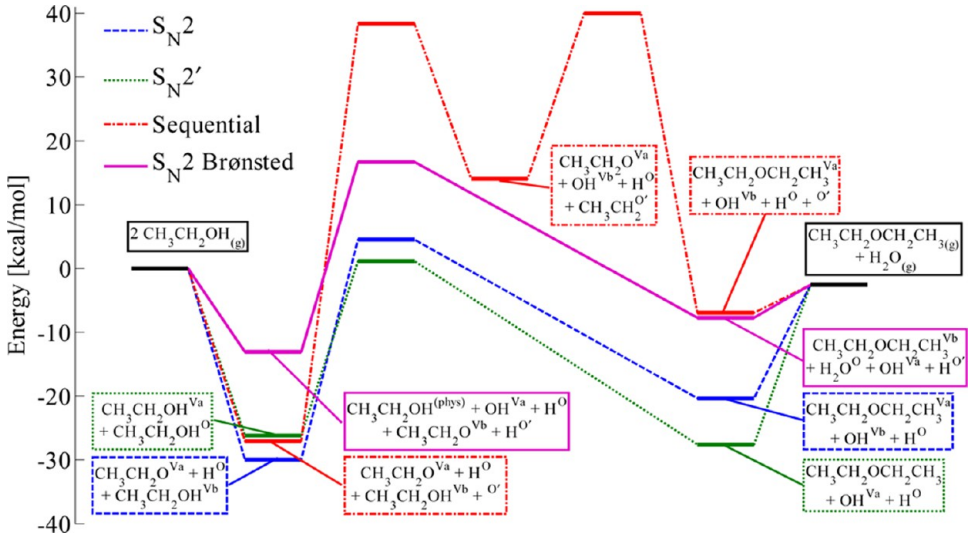

Figure 7. Energy diagram of principal reaction pathways for diethyl ether formation from ethanol. Note that for the "S_N2 Brønsted" mechanism, dissociated water as "OH^{Va} + H^{O}" is considered to be preadsorbed on the Al_2O_3 slab and remains there at the end of the catalytic cycle. In this way, all pathways in the diagram have the same gas-phase reference.

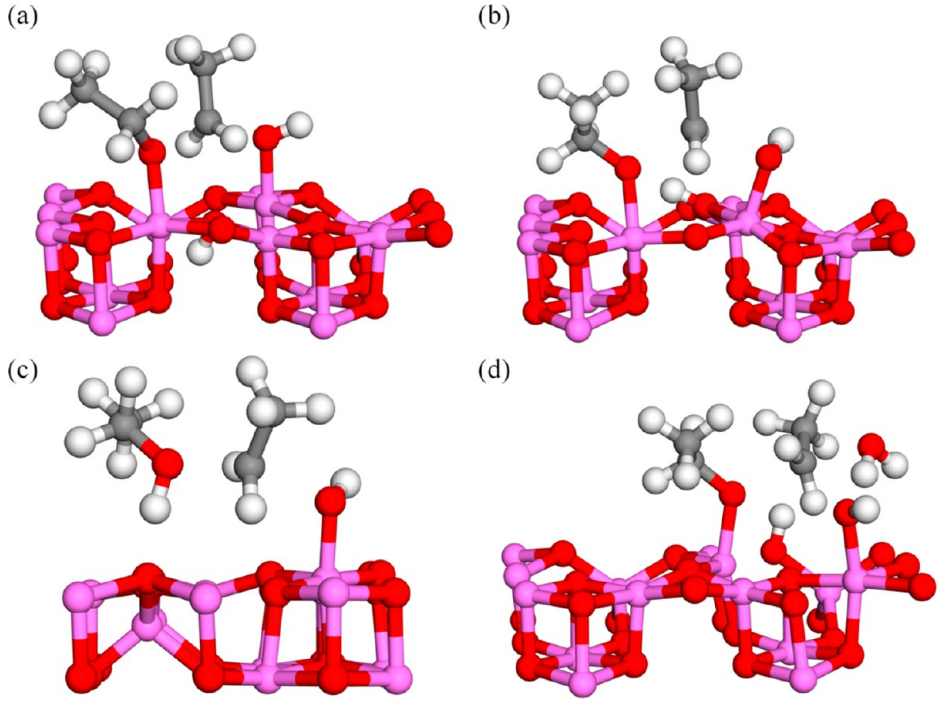

Figure 8. Transition state structures for diethyl ether production. See Supporting Information, Table S2 and the text for energetic information. (a) $CH_3CH_2O^{Va}$ + H^{O} + $CH_3CH_2OH^{Vb}$ → $CH_3CH_2OCH_2CH_3^{Va}$ + OH^{Vb} + H^{O} (R10), (b) $CH_3CH_2O^{Va}$ + H^{O} + $CH_3CH_2OH^{Vc}$ → $CH_3CH_2OCH_2CH_3^{Va}$ + OH^{Vc} + H^{O}, (c) $CH_3CH_2OH^{Va}$ + $CH_3CH_2OH^{O}$ → OH^{Va} + H^{O} + $CH_3CH_2OCH_2CH_3$ (R13), (d) $CH_3CH_2OH^{(phys)}$ + OH^{Va} + H^{O} + $CH_3CH_2O^{Vb}$ + $H^{O\prime}$ → $CH_3CH_2OCH_2CH_3^{Vb}$ + H_2O^{O} + OH^{Va} + $H^{O\prime}$ (R14).

dehydration barriers. The adsorption energies differ on sites V_a and V_b. As a result, the stability of the transition state should also be different for the barriers to be invariant with the adsorption site. However, the carbenium ion stability is the same in these two cases, so the remaining component contributing to the total energy of the transition state is the hydroxyl adsorption on the surface. The hydroxyl stability on sites V_a and V_b follows the stability of ethanol (the reactant) on these two sites, accounting for the invariance of the activation barrier with site.

We have treated so far dehydration reactions on the fully dehydrated (100) surface. However, alumina surfaces are often at least partially hydrated at reaction conditions.[35] Previous reports have discussed the effects of surface hydration on reactivity.[8,13,44,45] We have therefore examined (in connection with the E2 mechanism) the effect of using OH^{Vb} (rather than a surface O site) to extract the $^{\beta}H$ from $CH_3CH_2OH^{Va}$; the OH^{Vb} was formed by dissociating H_2O^{Vb}. The barrier was 37 kcal/mol, identical to the regular E2 case (R6), and consistent with the correlation to the carbenium ion stability (Figure 6(d)). We have also considered the effect of coadsorbed

dx.doi.org/10.1021/cs4002833 | ACS Catal. 2013, 3, 1965−1975

(spectator) water on the E2 mechanism by adsorbing ethanol on the V_b site with dissociated water in its most stable position on the V_a site (OH^{Va} + H^O; note that during optimization H_2O^{Va} was reformed). The barrier of this elementary step is 33 kcal/mol (see Supporting Information, Figure S2(e) for transition state) and is slightly lower than the barrier of 36 kcal/mol in the absence of coadsorbed water, which suggests that water may reduce slightly the dehydration barrier. On the other hand, the adsorption calculations in this work and previous experimental studies[11,13] indicate that water also competes with ethanol for adsorption sites. In particular, steady-state experiments of DeWilde et al. demonstrate that increasing the amount of water cofed with a constant ethanol feed results in a monotonic decrease in the reaction rate.[13] This suggests that water does not enhance the reaction rate of ethanol dehydration. In addition to the foregoing studies, possible catalytic effects of H^O when water blocks Al sites were explored using ethanol adsorbed on a dissociated water molecule (OH^{Va} + H^O) in its most stable configuration on the V_a site (R9). The H^O attacks the O atom of ethanol (forming physisorbed water) as the C−O bond breaks and the $^{\beta}H$ is abstracted by a surface O site (Figure 6(e)). The barrier for this pathway is ∼13 kcal/mol higher than when ethanol is adsorbed directly on the V_a site, and this is at least partially related to the fact that water is only physisorbed rather than chemisorbed. The reactant configuration is not very stable either. As reported in Figure 2, the ethanol adsorption energy ΔE_{ads} = −6 kcal/mol on dissociated water, compared to −19 kcal/mol on the V_a site. In this type of mechanism, the H^O is acting as a Brønsted acid. Therefore this result suggests that, at least on the (100) facet, catalysis of ethanol dehydration to ethylene by a Brønsted-like site does not appear to be a favorable pathway.

To conclude this section, we briefly note that one potential side reaction of ethanol is dehydrogenation to acetaldehyde, typically observed only in low yields.[46] The computed dehydrogenation barrier for acetaldehyde formation from $CH_3CH_2O^{Va}$ is 45 kcal/mol (Figure 6(f)), which is 8 kcal/mol larger than the barrier for the E2 dehydration of ethanol. The alternative dehydrogenation sequence starting from ethanol (to form $CH_3CHOH^{Va\text{-}Vc}$) was found to be thermodynamically unfavorable (ΔE_{rxn} = 28 kcal/mol) and therefore the barrier was not computed. These observations rationalize the lack of selectivity to acetaldehyde over γ-Al_2O_3.

Diethyl Ether Formation. Elimination reactions (like those discussed for ethylene formation) are known to compete with substitution reactions.[47] Alcohols participate in nucleophilic substitution, and therefore multiple variants of S_N2 reactions have been examined, beginning with Lewis sites. The energetics of the principal pathways are summarized in Figure 7. The adsorption calculations indicate that $CH_3CH_2O^{Va}$ + H^O is more stable than ethanol on V_a sites (by 3 kcal/mol), while ethanol is more stable than $CH_3CH_2O^{Va}$ + H^O on V_b sites (by 2 kcal/mol). This is adopted as the primary configuration, and a barrier of 35 kcal/mol for the formation of diethyl ether was found. As shown in Figure 8(a), $CH_3CH_2O^{Va}$ on the V_a site acts as the attacking nucleophile to which the ethyl group of ethanol is transferred, and the OH^{Va} fragment of ethanol is ejected as the leaving group. The nucleophile and leaving group interact with the attacked carbon atom from opposite sites (∼145° O−C−O bond angle). At the transition state, the H-$^{\alpha}$C−H bond angle of the transferring fragment is close to 120°, indicative of sp^2 hybridization. The C−C bond axis is oriented normal to the surface to minimize repulsion and maximize the stabilizing interactions between the $^{\alpha}$C and the O atoms of both $CH_3CH_2O^{Va}$ and OH^{Va}. All of these observations are consistent with a classic S_N2 mechanism and specifically the backside route of attack. We refer to this pathway as (R10) in Figure 4 and as "S_N2" in Figure 7. Other configurations of the reactants were also examined, including swapping the positions of ethoxy and ethanol on the V_a and V_b sites, and also adsorbing ethoxy on V_a and ethanol on V_c. In the former case, the barrier was 31 kcal/mol which is lower than the barrier of (R10), but the adsorbates are not as stable in these sites. In the latter case, the barrier was ∼15 kcal/mol higher (i.e., 46 kcal/mol), with the V_c site significantly tilted at the transition state, and the O−C−O bond angle measuring ∼125° (Figure 8(b)). The V_a and V_c sites may be situated too close to one another to allow for the same transition state stabilization that occurs with the pairing of V_a and V_b sites. All of the foregoing S_N2 mechanisms involve a backside route of attack. It is also possible for a frontside nucleophilic attack to occur, but it is typically energetically unfavorable. To prove this, we have examined one frontside attack mechanism with ethanol on V_a and ethoxy on V_b (Supporting Information, Figure S2(f)), and found the barrier to be 55 kcal/mol, 20 kcal/mol higher than in the backside route of attack. This is consistent with homogeneous chemistry and also with observations of stereochemical inversion for ether formation from 2-butanol, which takes place during an S_N2 backside attack.[23] In addition, in analogy to our study on the E2 barrier (R6), we have explored the hydration effect on the S_N2 reaction (R10). We calculated the barrier for the case in which ethanol, ethoxy, and H are adsorbed in the same configurations as in (R10), while water is adsorbed on the V_c site. The barrier is reduced to 27 kcal/mol (see Supporting Information, Figure S2(g) for transition state) compared to 35 kcal/mol without coadsorbed water, suggesting that coadsorbed water may make the reaction more favorable. However, the aforementioned opposing effect because of competitive adsorption between water and ethanol applies here as well. Further, similar to ethylene formation, experimental diethyl ether formation rates decrease monotonically with increasing water cofeed.[13] Thus, water appears to inhibit rather than accelerate ether formation rates.

Additional postulated S_N2-type mechanisms involve alternative adsorption configurations for one of the ethanol molecules. In the first case, one of two ethanol molecules is adsorbed on a surface O site, rather than adsorbing both on Al centers (Figure 8(c)). Note that the O site may still be considered as a Lewis (base) site. This pathway is labeled (R13) in Figure 4 and "S_N2'" in Figure 7, and is similar to a mechanism proposed by Jain and Pillai.[21,22] Consistent with the adsorption calculations, this type of reactant state is less stable than when two Al centers are involved (see Figure 7), but the barrier is also low (27 kcal/mol) and therefore the reaction is plausible. A second case features one ethanol physisorbed on a dissociated water molecule via hydrogen bonding, while ethoxy is stabilized on a nearby V_b site (R14). The H^O of dissociated water, acting as a Brønsted acid, attacks the O of the physisorbed ethanol as the C−O bond dissociates while a new C−O bond forms between adsorbed ethoxy and the C_2H_5 fragment (see "S_N2 Brønsted" mechanism in Figure 7 and Figure 8(d)). The barrier is 30 kcal/mol, which is competitive with the lowest barrier pathways. However this configuration is less stable than the analogous state with ethanol adsorbed directly on the V_a site. Referenced to the slab with

$CH_3CH_2O^{Vb}$, OH^{Va}, and $2H^O$ preadsorbed, the ethanol adsorption energy is only −5 kcal/mol (compared to −19 kcal/mol for direct adsorption on the V_a site). The low adsorption energy suggests that this pathway may be less preferred than mechanisms with direct adsorption on Al sites. Considering the dependence of preferred adsorption states on condition-specific parameters (e.g., equilibrium constants and reactant partial pressures) and also the similarity of the Lewis- and Brønsted-catalyzed reaction barriers (30 vs 35 kcal/mol), it is difficult in this case to determine the dominant pathway from the DFT information alone. We therefore couple our theoretical observations with recent experimental evidence. DeWilde et al. measured KIEs on ethanol dehydration over γ-Al_2O_3 using deuterated ethanol feeds, and did not observe any statistically significant effect on diethyl ether formation rates.[13] Isotopic scrambling of adsorbed H is expected given the low O−H dissociation barriers reported in this study. As a result, a KIE should be observed if the Brønsted-catalyzed pathway is dominant because O−H dissociation is part of the mechanism. Since no isotope effect is observed, we conclude that while Brønsted-catalyzed ether formation is possible, it is not expected to be a dominant pathway. Finally, we note at this point the possibility of two alkoxy molecules reacting to form ether. This type of reaction was proposed as the dominant pathway for dimethyl ether formation from methanol on γ-Al_2O_3(110).[10] Such a pathway involves the formation of an adsorbed O^{Al} species as one of the products, and we have found that this species is very unstable on the (100) surface (the nearby H^O prefers to recombine with the O^{Al} to form OH^{Al}). Therefore the pathway involving two ethoxys is not favorable on the (100) facet.

In the previous sets of pathways, a C−O bond breaks and a new C−O bond forms in the same elementary step. It is also plausible that these two bonds may break and form sequentially in two separate steps. Recall that the formation of $CH_3CH_2^O$ + OH^{Va} from ethanol was considered as an ethylene formation mechanism. The same step has been considered here again for ether formation but in the presence of ethoxy (R11), and we found it to exhibit an even higher barrier (66 kcal/mol, versus 52 kcal/mol without ethoxy). The barrier for the second step (R12) is low, E_a = 26 kcal/mol (Supporting Information, Figure S2(h)-(i); "Sequential" pathway in Figure 7). The higher barrier in the presence of ethoxy is partly because the mechanism takes place on a different site (V_b rather than V_a). When instead ethanol is adsorbed on the stronger V_a acid site and dissociates to $CH_3CH_2^O$ + OH^{Va} (with ethoxy on the V_b site), the barrier is 59 kcal/mol. Another contributing effect may be electron withdrawal from the surface by the ethoxy, leading to decreased basicity of the surface O on which $CH_3CH_2^O$ adsorbs and decreased stability at the transition state. We have also tested the barriers of some ethylene formation mechanisms (e.g., the E2 mechanism) and found that the barriers were not significantly affected by the presence of another adsorbed ethanol. In summary, we find that single-step mechanisms for diethyl ether formation are preferred over a two-step mechanism via a $CH_3CH_2^O$ intermediate, and that the transition state structures of the most favorable pathways are consistent with an S_N2 mechanism.

Decomposition of Diethyl Ether to Ethylene. In a previous section, we discussed pathways leading from ethanol and related C2 intermediates to ethylene. There is also evidence that ethylene forms from the decomposition of diethyl ether. Knözinger and Köhne have performed a series of ethanol dehydration experiments at fixed temperatures with varying residence time.[18] At an intermediate temperature (571 K), a maximum in ether production as a function of residence time was observed. Since the ethanol pressure continues to drop, they concluded that at least some of the ethylene forms via decomposition of ether.[18] To corroborate this result, we investigated the decomposition of diethyl ether via both "$E1^E$" (R16) and "$E2^E$" (R15) mechanisms (Figure 9(a)−(b)); superscript "E" denotes that the elimination takes place from diethyl ether). These pathways are highly analogous to the E1′ and E2 mechanisms identified for direct ethylene formation from ethanol, since the H atom in the alcohol group of ethanol is simply substituted with an ethyl group for the case of diethyl ether. The barriers for the $E2^E$ and $E1^E$ mechanisms are 38 and 52 kcal/mol, respectively. These values are both within 1 kcal/mol of the corresponding ethanol dehydration mechanisms. This indicates that competition between ethylene formation from ethanol and from diethyl ether may exist depending on the relative partial pressures of ethanol and diethyl ether, which are dictated from the specific reaction conditions.

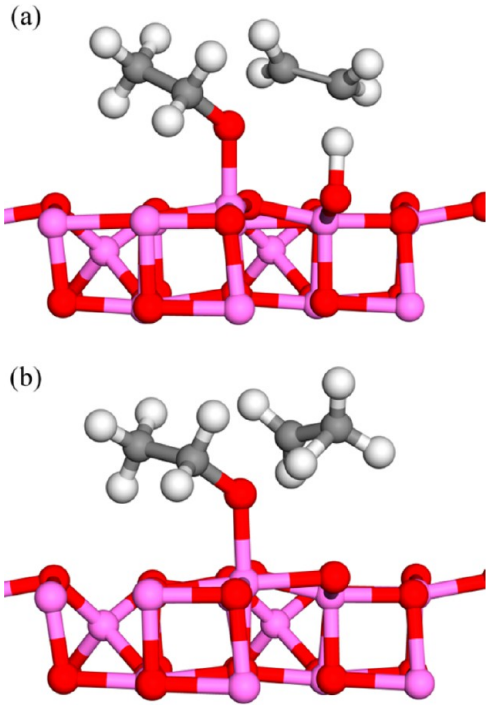

Figure 9. Transition state structures for ethylene formation from diethyl ether. See Supporting Information, Table S2 and the text for energetic information. (a) $CH_3CH_2OCH_2CH_3^{Va}$ + ^{O} → C_2H_4 + $CH_3CH_2O^{Va}$ + H^O (R15), (b) $CH_3CH_2OCH_2CH_3^{Va}$ → C_2H_4 + $CH_3CH_2OH^{Va}$ (R16).

Insights into Selectivity for Alkenes and Ethers. As demonstrated in this work, on the most stable sites of the (100) surface, the lowest barrier for ethylene formation is 37 kcal/mol, while diethyl ether is formed with a barrier of 35 kcal/mol in the most favorable path (from the most stable set of reactants). These values are similar, indicating some possible preference to ether at low temperatures. This preference is enhanced when hydration effects on the rate constants are considered. We showed in previous sections how the E2 and S_N2 reaction barriers decrease in the presence of coadsorbed (spectator) H_2O. With coadsorbed H_2O, the E2 barrier was

dx.doi.org/10.1021/cs4002833 | ACS Catal. 2013, 3, 1965−1975

lowered by 3 kcal/mol and the S_N2 barrier by 8 kcal/mol, resulting in a larger barrier difference of the E2 and S_N2 reactions. Thus, although water is experimentally shown to inhibit the absolute reaction rates for both mechanisms, these results suggest a possible reason for the higher rate of etherification relative to dehydration at low temperatures (488 K).[17,18] So far we have discussed rate constants, however coverages are also important. To illustrate this, we consider here rate expressions for the key reaction steps in the limit of low conversion so that the reverse rates are negligible. At low temperatures, higher coverages of ethanol and ethoxy cover the surface, favoring the etherification reaction

$$r_{S_N2} = k_{S_N2}[CH_3CH_2OH^{Al}][CH_3CH_2O^{Al}]$$

At higher temperatures, more surface vacant sites are exposed at the expense of ethanol and ethoxy, and high coverages of vacant sites promote dehydration rates

$$r_{E2} = k_{E2}[CH_3CH_2OH^{Al}][^{\circ}]$$

This leads to an increase in the relative rate of dehydration compared to etherification with increasing reaction temperature. This is consistent with experimental observations of primarily ether formation at low temperature (488 K) and primarily olefin formation at higher temperatures (616 K).[17,18] It is also consistent with a "crossover" regime characterized by simultaneous ether and alkene production, from not only ethanol[13,17,18,46] but also larger primary alcohols.[17,18] Thus, our calculations and subsequent analysis provide fundamental insights into the mechanistic origins of competition between dehydration and etherification of alcohols on γ-Al_2O_3.

CONCLUSIONS

The ethanol reaction network on γ-Al_2O_3(100) has been systematically examined using DFT. Ethanol and water adsorb competitively on Lewis sites, consistent with previous reports that water strongly inhibits alcohol dehydration. Adsorption of ethanol on surface Brønsted sites (ΔE_{ads} = −6 kcal/mol) is much weaker than on Lewis sites (ΔE_{ads} = −10 to −19 kcal/mol, depending on site). As a result, Brønsted-catalyzed mechanisms for ethanol dehydration and etherification are less favorable than Lewis-catalyzed pathways. Stability of ethanol and/or water adsorbates are not affected by coadsorption on this facet. Both concerted and sequential dehydration pathways to ethylene are examined, and a concerted E2 mechanism is the lowest energy pathway

$$CH_3CH_2OH^{Al} + {}^{O} \xrightarrow{E_a=37\,kcal/mol} C_2H_4 + OH^{Al} + H^{O}$$

Ethylene may also form from decomposition of diethyl ether, via elimination mechanisms analogous to those proposed for ethanol. The $E2^E$ is the most favorable pathway

$$CH_3CH_2OCH_2CH_3{}^{Al} + {}^{O} \xrightarrow{E_a=38\,kcal/mol} C_2H_4 + CH_3CH_2O^{Al} + H^{O}$$

Multiple routes to diethyl ether formation via S_N2 backside attack mechanisms are revealed. The lowest energy pathway is

$$CH_3CH_2O^{Al} + H^{O} + CH_3CH_2OH^{Al} \xrightarrow{E_a=35\,kcal/mol} CH_3CH_2OCH_2CH_3{}^{Al} + OH^{Al} + H^{O}$$

Consistent with observed selectivity trends for primary alcohols, ether and ethylene formation are energetically competitive while ethanol dehydrogenation to acetaldehyde has higher barriers. Coadsorbed (spectator) water lowers the S_N2 reaction barrier more than the E2 barrier, while low reaction temperatures are consistent with high coverages of ethanol and ethoxy. These observations are consistent with enhanced rates of diethyl ether formation relative to ethylene formation at low temperatures.

ASSOCIATED CONTENT

Supporting Information

Tables with information about coadsorbate stabilization, a table and figure with information on ethanol adsorption properties on O sites of γ-Al_2O_3, a table of elementary steps considered in the ethanol reaction network, and figures displaying additional transition state structures. This material is available free of charge via the Internet at http://pubs.acs.org.

AUTHOR INFORMATION

Corresponding Author

*E-mail: vlachos@udel.edu. Phone: 302-831-2830.

Notes

The authors declare no competing financial interest.

ACKNOWLEDGMENTS

M.A.C.'s and D.G.V.'s work was funded by the National Science Foundation (NSF) under Grant EFRI-937706. The supervisory contribution of G.M. was financially supported as part of the Catalysis Center for Energy Innovation, an Energy Frontier Research Center funded by the U.S. Department of Energy, Office of Science, Office of Basic Energy Sciences under Award No. DE-SC0001004. The authors acknowledge computational resources of the Extreme Science and Engineering Discovery Environment (XSEDE), which is supported by National Science Foundation Grant OCI-1053575. In connection with XSEDE, the computations were performed on high performance computing clusters administered by the Texas Advanced Computing Center (TACC) and on the Kraken cluster administered by the National Institute for Computational Sciences (NICS). M.A.C. is grateful to Jonathan Sutton and Vassili Vorotnikov for useful discussions.

REFERENCES

(1) Ross, J. *Heterogeneous Catalysis*; Elsevier: Amsterdam, The Netherlands, 2012; pp 71−75.
(2) *Wiley Critical Content - Petroleum Technology*; John Wiley & Sons: Hoboken, NJ, 2007; Vols. *1*−*2*, pp 502−504.
(3) *Wiley Critical Content - Petroleum Technology.*; John Wiley & Sons: Hoboken, NJ, 2007; Vols. *1*−*2*, pp 876−886.
(4) Hightower, J. W.; Hall, W. K. *Trans. Faraday Soc.* **1970**, *66*, 477−489.
(5) Knözinger, H. *Angew. Chem., Int. Ed. Engl.* **1968**, *7* (10), 791−805.
(6) Guo, N.; Caratzoulas, S.; Doren, D. J.; Sandler, S. I.; Vlachos, D. G. *Energy Environ. Sci.* **2012**, *5* (5), 6703−6716.
(7) Dabbagh, H. A.; Zamani, M.; Davis, B. H. *J. Mol. Catal. A: Chem.* **2010**, *333* (1−2), 54−68.
(8) Kwak, J. H.; Mei, D. H.; Peden, C. H. F.; Rousseau, R.; Szanyi, J. *Catal. Lett.* **2011**, *141* (5), 649−655.
(9) Kwak, J. H.; Rousseau, R.; Mei, D.; Peden, C. H. F.; Szanyi, J. *ChemCatChem* **2011**, *3* (10), 1557−1561.
(10) Zuo, Z.; Huang, W.; Han, P.; Gao, Z.; Li, Z. *Appl. Catal., A* **2011**, *408* (1−2), 130−136.
(11) Roy, S.; Mpourmpakis, G.; Hong, D.-Y.; Vlachos, D. G.; Bhan, A.; Gorte, R. J. *ACS Catal.* **2012**, *2* (9), 1846−1853.
(12) Kovarik, L.; Genc, A.; Wang, C.; Qiu, A.; Peden, C. H. F.; Szanyi, J.; Kwak, J. H. *J. Phys. Chem. C* **2013**, *117* (1), 179−186.
(13) DeWilde, J. F.; Chiang, H.; Hickman, D. A.; Ho, C. R.; Bhan, A. *ACS Catal.* **2013**, *3* (4), 798−807.
(14) Liu, X.; Truitt, R. E. *J. Am. Chem. Soc.* **1997**, *119* (41), 9856−9860.

(15) Pines, H.; Haag, W. O. *J. Am. Chem. Soc.* **1960**, *82* (10), 2471−2483.
(16) Knözinger, H.; Bühl, H.; Kochloefl, K. *J. Catal.* **1972**, *24* (1), 57−68.
(17) Knözinger, H.; Köhne, R. *J. Catal.* **1964**, *3* (6), 559−560.
(18) Knözinger, H.; Köhne, R. *J. Catal.* **1966**, *5* (2), 264−270.
(19) Knözinger, H.; Scheglila, A. *J. Catal.* **1970**, *17* (2), 252−263.
(20) Shi, B. C.; Dabbagh, H. A.; Davis, B. H. *Top. Catal.* **2002**, *18* (3−4), 259−264.
(21) Jain, J. R.; Pillai, C. N. *Tetrahedron Lett.* **1965**, *6* (11), 675−678.
(22) Jain, J. R.; Pillai, C. N. *J. Catal.* **1967**, *9* (4), 322−330.
(23) Shi, B. C.; Davis, B. H. *J. Catal.* **1995**, *157* (2), 359−367.
(24) Wischert, R.; Coperet, C.; Delbecq, F.; Sautet, P. *Chem. Commun.* **2011**, *47* (17), 4890−4892.
(25) Kwak, J. H.; Hu, J. Z.; Kim, D. H.; Szanyi, J.; Peden, C. H. F. *J. Catal.* **2007**, *251* (1), 189−194.
(26) Kresse, G.; Hafner, J. *Phys. Rev. B: Condens. Matter Mater. Phys.* **1993**, *47* (1), 558−561.
(27) Kresse, G.; Hafner, J. *Phys. Rev. B: Condens. Matter Mater. Phys.* **1994**, *49* (20), 14251−14269.
(28) Kresse, G.; Furthmüller, J. *Comput. Mater. Sci.* **1996**, *6* (1), 15−50.
(29) Kresse, G.; Furthmüller, J. *Phys. Rev. B: Condens. Matter Mater. Phys.* **1996**, *54* (16), 11169−11186.
(30) Perdew, J. P.; Wang, Y. *Phys. Rev. B: Condens. Matter Mater. Phys.* **1992**, *45* (23), 13244−13249.
(31) Perdew, J. P.; Chevary, J. A.; Vosko, S. H.; Jackson, K. A.; Pederson, M. R.; Singh, D. J.; Fiolhais, C. *Phys. Rev. B: Condens. Matter Mater. Phys.* **1992**, *46* (11), 6671−6687.
(32) Blöchl, P. E. *Phys. Rev. B: Condens. Matter Mater. Phys.* **1994**, *50* (24), 17953−17979.
(33) Kresse, G.; Joubert, D. *Phys. Rev. B: Condens. Matter Mater. Phys.* **1999**, *59* (3), 1758−1775.
(34) Krokidis, X.; Raybaud, P.; Gobichon, A.-E.; Rebours, B.; Euzen, P.; Toulhoat, H. *J. Phys. Chem. B* **2001**, *105* (22), 5121−5130.
(35) Digne, M.; Sautet, P.; Raybaud, P.; Euzen, P.; Toulhoat, H. *J. Catal.* **2004**, *226* (1), 54−68.
(36) Henkelman, G.; Jónsson, H. *J. Chem. Phys.* **1999**, *111* (15), 7010−7022.
(37) Henkelman, G.; Uberuaga, B. P.; Jonsson, H. *J. Chem. Phys.* **2000**, *113* (22), 9901−9904.
(38) Ide, M. S.; Hao, B.; Neurock, M.; Davis, R. J. *ACS Catal.* **2012**, *2* (4), 671−683.
(39) Schneider, W. F.; Hass, K. C.; Miletic, M.; Gland, J. L. *J. Phys. Chem. B* **2002**, *106* (30), 7405−7413.
(40) Mei, D.; Ge, Q.; Szanyi, J.; Peden, C. H. F. *J. Phys. Chem. C* **2009**, *113* (18), 7779−7789.
(41) Metiu, H.; Chrétien, S.; Hu, Z.; Li, B.; Sun, X. *J. Phys. Chem. C* **2012**, *116* (19), 10439−10450.
(42) Tang, W.; Sanville, E.; Henkelman, G. *J. Phys.: Condens. Matter* **2009**, *21* (8), 084204.
(43) Joubert, J.; Fleurat-Lessard, P.; Delbecq, F.; Sautet, P. *J. Phys. Chem. B* **2006**, *110* (14), 7392−7395.
(44) Wischert, R.; Copéret, C.; Delbecq, F.; Sautet, P. *Angew. Chem., Int. Ed.* **2011**, *50* (14), 3202−3205.
(45) Wischert, R.; Laurent, P.; Copéret, C.; Delbecq, F.; Sautet, P. *J. Am. Chem. Soc.* **2012**, *134* (35), 14430−14449.
(46) Basagiannis, A.; Panagiotopoulou, P.; Verykios, X. *Top. Catal.* **2008**, *51* (1−4), 2−12.
(47) Loudon, G. M. *Organic Chemistry*., 4th ed.; Oxford University Press: New York, 2002.